Article

Cell Reports

Rapid and Efficient Direct Conversion of Human Adult Somatic Cells into Neural Stem Cells by HMGA2/let-7b

Graphical Abstract

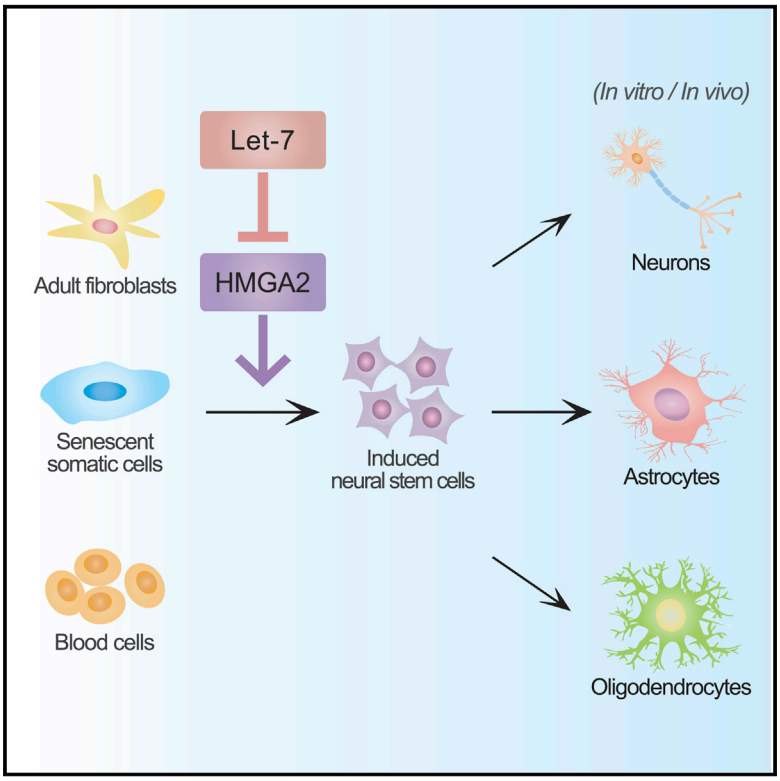

Highlights

- Inhibition of let-7 promotes direct reprogramming and self-renewal of hiNSCs
- HMGA2, a target of let-7, promotes the rapid and efficient generation of hiNSCs
- HMGA2 facilitates the direct reprogramming of human senescent cells and blood cells

Authors

Kyung-Rok Yu, Ji-Hee Shin, ..., Dong Wook Han, Kyung-Sun Kang

Correspondence

kangpub@snu.ac.kr

In Brief

Efficient generation of induced neural stem cells (iNSCs) from human somatic cells has remained challenging. Here, Yu et al. show that inhibition of the let-7 microRNA, or expression of its target HMGA2, facilitates SOX2-mediated direct reprogramming of human adult fibroblasts, senescent somatic cells, and blood cells into iNSCs. These hiNSCs display tridifferentiation ability and functionality, which could potentially provide therapeutic treatment for diverse neurological diseases.

Accession Numbers

GSE59301

Yu et al., 2015, Cell Reports *10*, 441–452
January 20, 2015
http://dx.doi.org/10.1016/j.celrep.2014.12.038

Cell Reports
Article

Rapid and Efficient Direct Conversion of Human Adult Somatic Cells into Neural Stem Cells by HMGA2/let-7b

Kyung-Rok Yu,[1,2,9] Ji-Hee Shin,[1,2,9] Jae-Jun Kim,[1,2,9] Myung Guen Koog,[1,2] Jin Young Lee,[1,2] Soon Won Choi,[1,2] Hyung-Sik Kim,[1,2] Yoojin Seo,[1,2] SeungHee Lee,[1,2,3] Tae-hoon Shin,[1,2] Min Ki Jee,[1,2] Dong-Wook Kim,[4] Sung Jun Jung,[5] Sue Shin,[6,7] Dong Wook Han,[8] and Kyung-Sun Kang[1,2,*]

[1]Adult Stem Cell Research Center, College of Veterinary Medicine, Seoul National University, Seoul 151-742, Korea
[2]The Research Institute for Veterinary Science, College of Veterinary Medicine, Seoul National University, Seoul 151-742, Korea
[3]Institute for Stem Cell and Regenerative Medicine in Kang Stem Biotech, Biotechnology Incubating Center, Seoul National University, Seoul 151-742, Korea
[4]Department of Physiology and Brain Korea 21 Plus Project for Medical Science, Yonsei University College of Medicine, Seoul 120-752, Korea
[5]Department of Physiology, School of Medicine, Hanyang University, Seoul 133-791, Korea
[6]Department of Laboratory Medicine, SMG-SNU Boramae Medical Center, Seoul National University College of Medicine, Seoul 156-707, Korea
[7]Seoul Metropolitan Public Cord Blood Bank, Allcord, Seoul 156-707, Korea
[8]Department of Stem Cell Biology, School of Medicine, Konkuk University, Seoul 143-701, Korea
[9]Co-first author
*Correspondence: kangpub@snu.ac.kr
http://dx.doi.org/10.1016/j.celrep.2014.12.038

SUMMARY

A recent study has suggested that fibroblasts can be converted into mouse-induced neural stem cells (miNSCs) through the expression of defined factors. However, successful generation of human iNSCs (hiNSCs) has proven challenging to achieve. Here, using microRNA (miRNA) expression profile analyses, we showed that let-7 microRNA has critical roles for the formation of PAX6/NESTIN-positive colonies from human adult fibroblasts and the proliferation and self-renewal of hiNSCs. *HMGA2*, a let-7-targeting gene, enables induction of hiNSCs that displayed morphological/molecular features and in vitro/in vivo differentiation potential similar to H9-derived NSCs. Interestingly, HMGA2 facilitated the efficient conversion of senescent somatic cells or blood CD34+ cells into hiNSCs through an interaction with SOX2, whereas other combinations or SOX2 alone showed a limited conversion ability. Taken together, these findings suggest that HMGA2/let-7 facilitates direct reprogramming toward hiNSCs in minimal conditions and maintains hiNSC self-renewal, providing a strategy for the clinical treatment of neurological diseases.

INTRODUCTION

Direct lineage conversion strategies have been developed for the conversion of animal and human somatic cells into other lineage-specific cells to overcome the issues of induced pluripotent stem cells (iPSCs). However, these direct reprogramming technologies have limitations, as these lineage-specific cells are fully differentiated with limited proliferation potential and are difficult to use for transplantation or clinical trials. Recently, it has been reported that neural stem cells can be successfully generated through defined factors in mouse fibroblasts (Han et al., 2012; Thier et al., 2012). Because directly converted neuronal cell populations are heterogeneous and unable to proliferate, the derivation of neural stem cells (NSCs) is desired to obtain sufficient amounts of cells with relatively safe and homogeneous cell populations. More recently, Ring et al. (2012) reported that SOX2 is sufficient to generate mouse induced NSCs (iNSCs) from mouse embryonic fibroblasts. However, the direct conversion of human adult somatic cells into human iNSCs (hiNSCs) has not been well characterized yet.

High-mobility group A2 (HMGA2) is an architectural transcription factor that potentiates the effects of transcription factors through alterations of chromatin structures, reflecting binding to the minor groove of AT-rich DNA sequences (Reeves, 2001). Hmga2 overexpression elevates self-renewal activity in purified hematopoietic stem cells (Copley et al., 2013) and rescues the in vitro aging process of mesenchymal stem cells (MSCs) (Yu et al., 2013). Hmga2 is highly expressed in fetal NSCs, but its expression gradually declines with age. Hmga2 promotes the self-renewal of NSCs through the repression of $p16^{Ink4a}$ and $p19^{Arf}$ (Nishino et al., 2008). Furthermore, HMGA2 is essential for the open chromatin state of neural precursor cells (NPCs) at early developmental stages and facilitates the reprogramming of late-stage NPCs into cells with early stage-specific capacities (Kishi et al., 2012).

Lethal-7 (let-7) microRNAs (miRNAs) target *HMGA2*, which contains seven target sites in its 3′ UTR, and these miRNAs show inverse expression patterns during fetal development

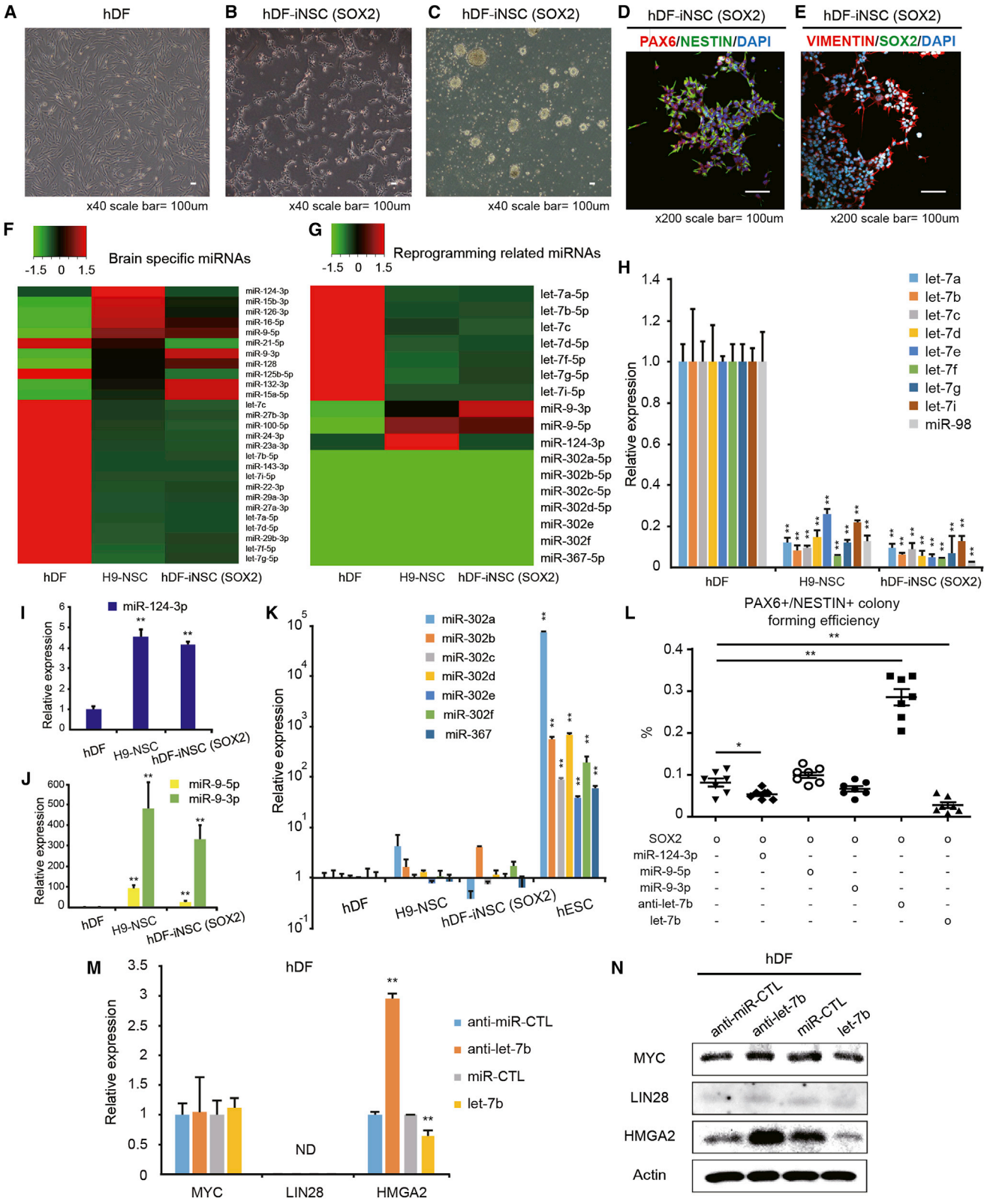

(legend on next page)

and adult aging (Fusco and Fedele, 2007). Recent studies have shown that let-7 miRNAs are involved in the regulation of the nervous system, including neural cell specification and self-renewal regulation in NSCs (Rybak et al., 2008; Zhao et al., 2010). However, the effects of HMGA2 and let-7 on the direct reprogramming of human fibroblasts into hiNSCs remain unknown. Here, we report that overexpressing HMGA2/anti-let-7b in combination with SOX2 facilitated direct reprogramming of human somatic cells toward hiNSCs.

RESULTS

Expression Profiling and Validation of miRNAs in hiNSCs

hiNSCs were generated from adult human dermal fibroblasts (hDFs) using methods described previously with modifications (Ring et al., 2012). Briefly, hDFs cultured with STO feeder cells on poly-L-ornithine (PLO) and fibronectin (FN)-coated glass coverslips were infected with retroviral *SOX2*. NSC-like colonies were generated from SOX2-transduced hDFs within 2 or 3 weeks of infection. These colonies were collected and cultured as neurospheres for three or four passages. The neurospheres were seeded and grown as a monolayer, and the neurosphere culture procedures were repeated at least three times to generate a homogenous population of hiNSCs. SOX2-transduced hiNSCs expressed NSC-specific markers, such as PAX6, NESTIN, VIMENTIN, and SOX2, and had a morphology similar to H9-derived NSCs (H9-NSCs) (Figures 1A–1E and S2A).

We next determined the miRNA profiles of hDFs, H9-NSCs, and SOX2-transduced hiNSCs through microarray analyses. To examine whether SOX2-transduced hiNSCs exhibit a neuronal identity, we selected brain-specific miRNAs from the microarray data set. The brain-specific miRNA expression pattern of SOX2-transduced hiNSCs was more similar to that of H9-NSCs than hDFs (Figure 1F); however, a subset of miRNAs expressing similar patterns in hiNSCs and hDFs was also detected, likely reflecting residual epigenetic memory. Previously, a role for let-7, miR-9, and miR-124 in the control of NSC maintenance and direct reprogramming process has been reported (Kawahara et al., 2012; Yoo et al., 2011; Zhao et al., 2010). Therefore, we extracted reprogramming-related miRNAs from the microarray data set and validated them via quantitative real-time RT-PCR (qRT-PCR) (Figures 1G–1K). Interestingly, all let-7/miR-98 family members were downregulated in H9-NSCs and SOX2-transduced hiNSCs compared with hDFs (Figure 1H). It has been reported that neural lineage-specific miRNAs, such as miR-9-5p, miR-9-3p, and miR-124, play key roles in the conversion of fibroblasts into functional neurons (Xue et al., 2013; Yoo et al., 2011). The expression levels of miR-9-5p, miR-9-3p, and miR-124 were upregulated in H9-NSCs and SOX2-transduced hiNSCs compared with hDFs (Figures 1I and 1J). However, significant alterations in the expression levels of the embryonic-stem-cell-specific miR-302/miR-367 family were not detected between hDFs, H9-NSCs, and hiNSCs, whereas the abundant expression of these miRNAs was detected in human embryonic stem cells (hESCs) (Figure 1K).

Let-7b Regulates iNSC Reprogramming Efficiency and Self-Renewal

To determine whether miRNA activity promotes the reprogramming of hDFs into hiNSCs, we transfected miR-124, miR-9-5p, miR-9-3p, anti-let-7b, let-7b, or miR-CTL into SOX2-transduced cells. The overexpression of miR-124, miR-9-5p, and miR-9-3p did not enhance the production of PAX6/NESTIN-positive colonies. In the presence of these miRNAs, SOX2-transduced hDFs were converted into neuron-like cells rather than NSC-like colonies (data not shown). However, let-7b inhibition increased reprogramming efficiency approximately 3.5-fold over anti-miR-CTL, whereas let-7b overexpression significantly decreased reprogramming efficiency (Figure 1L). To gain insight into let-7 target genes, we analyzed let-7-relevant genes using ingenuity pathway analysis (IPA) software (Figures S1A–S1C). Among the top 15 IPA findings, we selected *MYC*, *LIN28*, and *HMGA2*, which are known NSC-related genes. To further assess the role of SOX2 and let-7 regulators on the expression of *MYC*, *LIN28*, and *HMGA2*, we transduced SOX2 into hDFs and investigated expression levels on days 3 and 7. We found that the expression of *MYC*, *LIN28*, *HMGA2*, and let-7b was not altered by the transduction of hDFs with SOX2 (Figures S1D and S1E). Furthermore, transfection with let-7b or anti-let-7b

Figure 1. Role of let-7b in hDF-iNSC Derivation

(A and B) Morphology of human dermal fibroblasts (hDFs) (A) and iNSCs derived from SOX2-transduced hDFs; (B) bright-field microscopy. The scale bar represents 100 μm.

(C) Bright-field image of early neurosphere-like colonies generated through SOX2 transduction. Neurosphere-like colonies were manually isolated, subjected to multiple passages for rounds of neurosphere generation, and grown in PLO/FN-coated culture dishes. The scale bar represents 100 μm.

(D and E) Immunocytochemistry analysis of NSC-specific marker proteins in hDF-iNSCs using antibodies against PAX6, NESTIN (D), and VIMENTIN, SOX2 (E). Nuclei were counterstained with DAPI. The scale bar represents 100 μm.

(F and G) Heatmap of brain-specific miRNAs (F) and reprogramming-related miRNAs (G) in hDFs, H9-NSCs, and hDF-iNSCs (SOX2).

(H) qRT-PCR analysis of let-7/miR-98 family expression in hDFs, H9-NSCs, and hDF-iNSCs (SOX2). Error bars denote the SD of triplicate reactions. $^{**}p < 0.01$.

(I and J) qRT-PCR validation of miR-124-3p (I) and miR-9-5p/miR-9-3p (J) in hDFs, H9-NSCs, and hDF-iNSCs (SOX2). Error bars denote the SD of triplicate reactions. $^{**}p < 0.01$.

(K) Relative expression levels of the ESC-specific miR-302/miR-367 family were measured through qRT-PCR in hDFs, H9-NSCs, hDF-iNSCs (SOX2), and hESCs. Error bars denote the SD of triplicate reactions. $^{**}p < 0.01$.

(L) The efficiency of PAX6- and NESTIN-positive colony formation was measured after the transfection of miR-124-3p, miR-9-5p, miR-9-3p, anti-let-7b, and let-7b into SOX2-transduced hDFs. Error bars denote the SD of seven separate assays. $^{*}p < 0.05$; $^{**}p < 0.01$.

(M and N) Relative expression levels of MYC, LIN28, and HMGA2 were measured by qRT-PCR (M) and western blotting (N) in anti-miR-CTL-, anti-let-7b-, miR-CTL-, and let-7b-transfected hDFs. Error bars denote the SD of triplicate reactions. $^{**}p < 0.01$.

See also Figure S1.

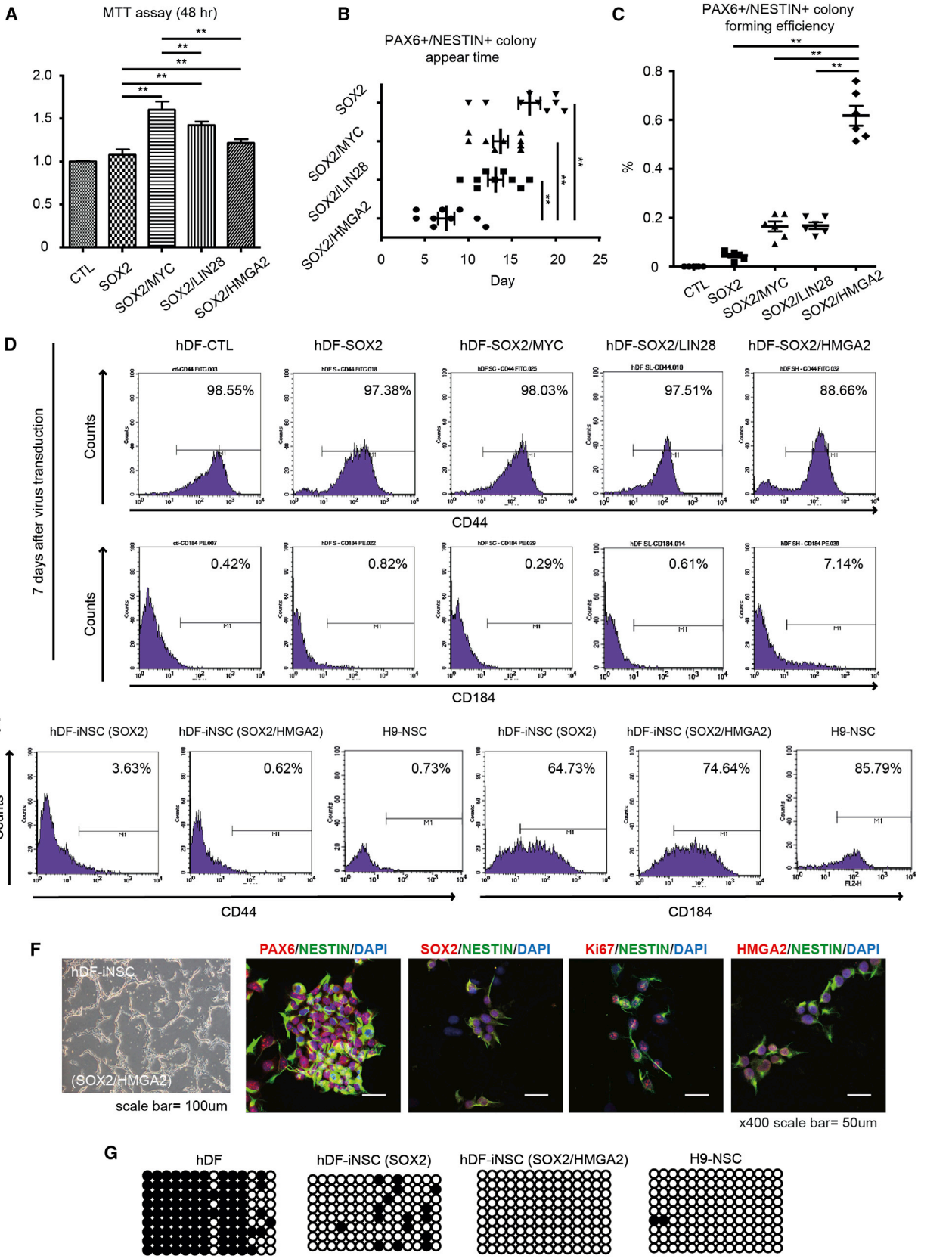

(legend on next page)

significantly regulated the expression level of HMGA2, but not MYC and LIN28, in hDFs, suggesting that HMGA2 expression was increased during the SOX2/anti-let-7b-mediated hiNSC reprogramming process (Figures 1M and 1N).

We next transfected let-7b into hiNSCs and measured cell proliferation through 5-bromodeoxyuridine (BrdU) labeling of dividing cells to determine whether let-7b regulates hiNSC proliferation. The transfection of let-7b decreased hiNSC proliferation in a dose-dependent manner, confirmed by the reduced percentage of BrdU-positive cells (Figures S1F and S1G). To assess whether let-7b regulates the self-renewal of hiNSCs, we performed a neurosphere-forming assay. Let-7b-transfected hiNSCs were smaller than miR-CTL-transfected hiNSCs and generated significantly fewer secondary neurospheres upon subcloning in response to increasing concentrations of let-7b (Figures S1H–S1J). These results demonstrated roles for let-7b in promoting reprogramming efficiency toward hiNSCs in combination with SOX2 and in regulating hiNSC proliferation and self-renewal.

The let-7b Target HMGA2 Promotes hiNSC Reprogramming

Previous studies and our IPA data have shown that let-7 expression inversely correlates with expression of *MYC*, *LIN28*, and *HMGA2* (Mayr et al., 2007; Rybak et al., 2008; Sampson et al., 2007). Here, we demonstrated that the overexpression of MYC, LIN28, and HMGA2 in combination with SOX2 increased cell proliferation compared with the overexpression of SOX2 alone. Among these factors, HMGA2 had the slightest effect on proliferation (Figure 2A). We examined whether MYC, LIN28, and HMGA2 in combination with SOX2 could promote reprogramming toward hiNSCs. Surprisingly, the expression of HMGA2 with SOX2 significantly increased reprogramming efficiency toward hiNSCs, as confirmed by PAX6/NESTIN-positive colony formation (Figure 2C). Furthermore, expressing HMGA2 with SOX2 shortened the time required for PAX6/NESTIN-positive colonies to appear from 17 days with SOX2 alone to 7.4 days with SOX2/HMGA2 overexpression (Figure 2B).

Immunophenotyping screens have revealed that a population of CD184+/CD271−/CD44−/CD24+ NSCs could be derived from human pluripotent stem cells (Yuan et al., 2011). Therefore, we used fluorescence-activated cell sorting to determine whether immunophenotyping alterations were induced at an early stage of reprogramming. Consistent with the data for the appearance of PAX6/NESTIN-positive colonies, only SOX2/HMGA2-overexpressing cells showed alterations in the cell population from CD44 positive to CD44 negative in approximately 10% of the total cells at 7 days postinfection. In addition, approximately 7% of the cell population was shifted from CD184 negative to CD184 positive (Figure 2D). The majority of hiNSCs and H9-NSCs showed CD44-negative and CD184-positive cell populations (Figure 2E). SOX2/HMGA2-transduced hiNSCs showed morphological features and NSC-specific marker expression that was similar to SOX2-transduced hiNSCs or H9-NSCs (Figure 2F). Next, we further examined NSC features among H9-NSCs, SOX2-transduced hiNSCs, SOX2/HMGA2-transduced hiNSCs, and SOX2/anti-let-7b-transduced hiNSCs. H9-NSCs and hiNSCs with different combinations showed similar expression patterns for PAX6, NESTIN, SOX2, Ki67, and HMGA2, which was confirmed by immunostaining (Figure S2A). At the transcriptional level, *SOX2*, *HMGA2*, *PAX6*, *NESTIN*, *MSI1*, and *GLAST* were induced in hiNSCs at a comparable level as H9-NSCs (Figure S2B). Under neuronal or glial differentiation conditions, H9-NSCs, SOX2-transduced hiNSCs, SOX2/HMGA2-transduced hiNSCs, and SOX2/anti-let-7b-transduced hiNSCs differentiated into neurofilament (NF)-positive neurons or glial fibrillary acidic protein (GFAP)-positive astrocytes, and a quantitative analysis demonstrated that the differentiation potential of SOX2/HMGA2-transduced hiNSCs was relatively higher for neurons and lower for astrocytes compared with H9-NSCs or hiNSCs in other combinations (Figure S2C).

We confirmed that SOX2/HMGA2-transduced hiNSCs could be stably maintained for more than 40 passages. The characteristic profile of late-passage SOX2/HMGA2-transduced hiNSCs (passage 48) was unchanged compared with early-passage SOX2/HMGA2-transduced hiNSCs (passage 8), as judged by NSC marker expression, nuclear size, and nuclear abnormalities (Figures S2D–S2F). Furthermore, NF-positive neurons or GFAP-positive astrocytes could be generated from both early- and late-passage SOX2/HMGA2-transduced hiNSCs, suggesting that these cells maintain a stable differentiation capability during continuous passaging. However, the neuronal differentiation potential was slightly decreased in late-passage hiNSCs, whereas the glial differentiation potential was slightly increased (Figures S2G and S2H).

We next assessed the *SOX2* DNA methylation status in hDFs, H9-NSCs, and SOX2- and SOX2/HMGA2-transduced hiNSCs. The methylation analysis of bisulfite-treated DNA showed that

Figure 2. Role of HMGA2 in hDF-iNSC Derivation

(A) The MTT cell proliferation assay was performed in hDF control, SOX2-, SOX2/MYC-, SOX2/LIN28-, and SOX2/HMGA2-transduced hDFs. Error bars denote the SD of triplicate assays. $^{**}p < 0.01$.

(B and C) The time of appearance (B) and efficiency of PAX6- and NESTIN-positive colony formation (C) were measured in control and SOX2-, SOX2/MYC-, SOX2/LIN28-, and SOX2/HMGA2-transduced hDFs. Error bars denote the SD of six or nine separate assays. $^{**}p < 0.01$.

(D) Flow cytometry analyses were performed with a negative cell surface marker of NSC, CD44, and a positive marker, CD184, in hDF control and SOX2-, SOX2/MYC-, SOX2/LIN28-, and SOX2/HMGA2-transduced hDFs at 7 days after virus transduction.

(E) Flow cytometry analysis for the negative NSC cell surface marker, CD44, and the positive NSC cell surface marker, CD184, in hDF-iNSCs (SOX2), hDF-iNSCs (SOX2/HMGA2), and H9-NSCs.

(F) Characterization of SOX2/HMGA2-transduced hDF-iNSCs. Morphology of hDF-iNSCs (SOX2/HMGA2) assessed using bright-field microscopy. Immunofluorescence images of hiNSCs using antibodies against PAX6, NESTIN, SOX2, Ki67, and HMGA2. The scale bars represent 100 or 50 μm.

(G) Methylation patterns of *SOX2* gene promoters were analyzed after bisulfite treatment of the DNA from hDFs, H9-NSCs, and hDF-iNSCs (SOX2 and SOX2/HMGA2). Filled and empty circles represent methylated and unmethylated CpGs, respectively.

See also Figure S2.

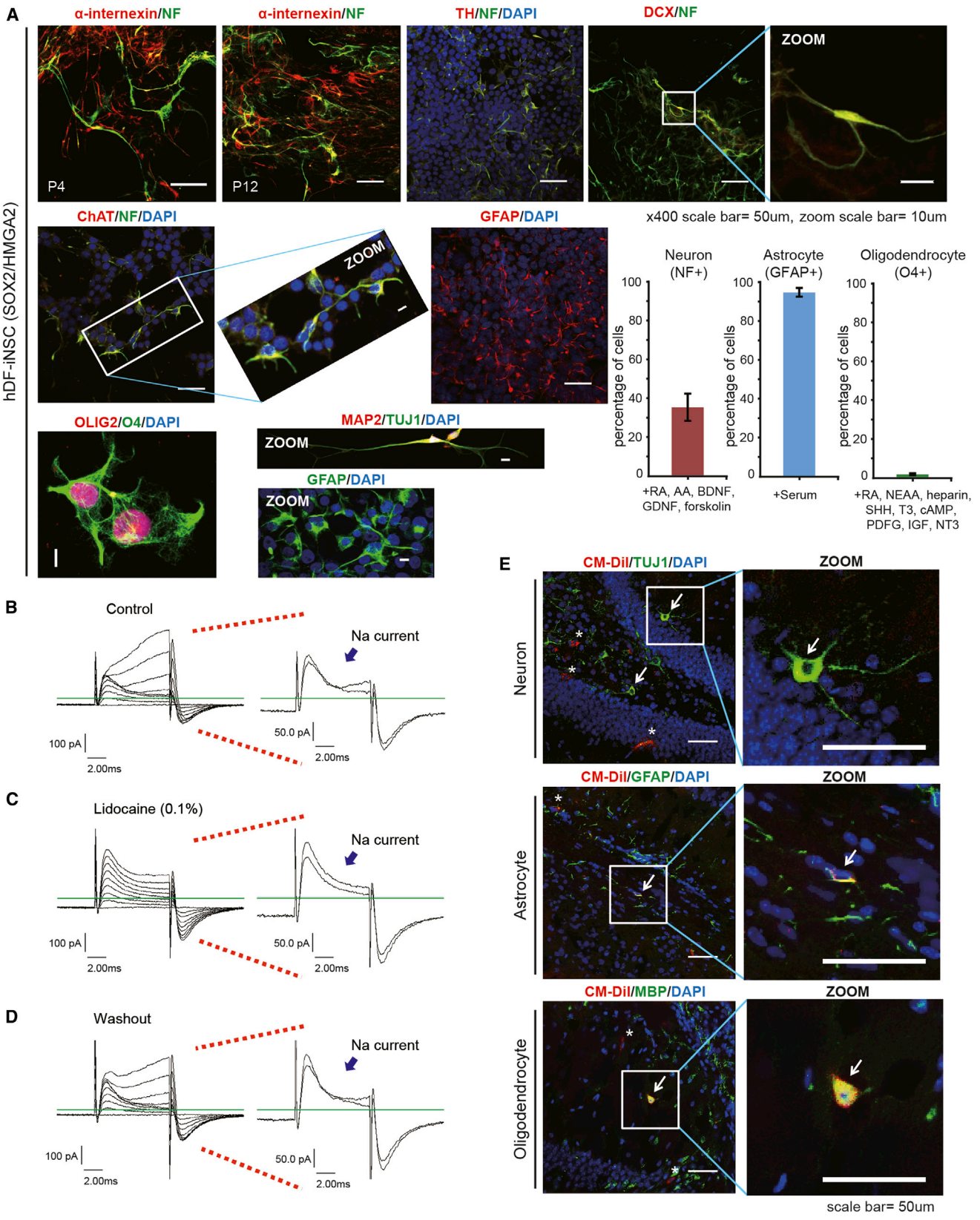

(legend on next page)

the hypomethylation of the *SOX2* promoter in hiNSCs was similar to that in H9-NSCs, suggesting that *SOX2* is transcriptionally activated (Figure 2G). These data indicate that the let-7b target HMGA2 significantly increases the efficiency and time of SOX2-induced reprogramming into hiNSCs, and SOX2/HMGA2-transduced hiNSCs showed characteristics similar to H9-NSCs in cell surface marker signatures, gene transcription levels, and methylation patterns.

Downregulation of HMGA2 Inhibits hiNSC Proliferation and Self-Renewal

To examine whether HMGA2 regulates hiNSC proliferation, we transfected hiNSCs with HMGA2-targeting small interfering RNA (siRNA) (siHMGA2) and measured cell proliferation using BrdU labeling of dividing cells. Downregulation of HMGA2 dramatically reduced the percentage of BrdU-positive cells (Figures S1K and S1L). Furthermore, siHMGA2-transfected hiNSCs showed a significantly reduced neurosphere size, confirmed by the diameter of neurospheres, and decreased self-renewal, confirmed by the number and percentage of cells generating secondary neurospheres among primary neurosphere (Figures S1M–S1O). Taken together, these results showed that the downregulation of HMGA2 with a siRNA against HMGA2 inhibits hiNSC proliferation and self-renewal.

hiNSCs Differentiate into Neurons, Astrocytes, and Oligodendrocytes

To examine the multipotency of hiNSCs, SOX2/HMGA2-transduced hiNSCs were differentiated into three main neural lineages: neurons, astrocytes, and oligodendrocytes. Subsequently, lineage-related markers were confirmed using immunocytochemistry. After 10–15 days of neuronal induction, immature neuronal markers; neuron-specific class III beta-tubulin (TUJ1) and doublecortin (DCX); and neuronal intermediate filaments, alpha-internexin (α-internexin) and NF, were detected (Figure 3A). Clonal analysis was performed to assess the self-renewal potential of hiNSCs. Neuronal differentiation was induced, and NF and alpha-internexin were stained in clones at multiple passages. After 10–25 days of neuronal induction, the mature neuronal marker, MAP2; the dopaminergic and noradrenergic neuron marker, tyrosine hydroxylase (TH); and the cholinergic neuron marker, choline acetyltransferase (ChAT), were expressed at similar levels compared with H9-NSCs (Figures 3A and S3A). The astrocytic differentiation of hiNSCs yielded GFAP-positive cells. Furthermore, cells double positive for the oligodendrocyte markers, O4 and OLIG2, were detected after 20–35 days of induction toward oligodendroglial fate. The various differentiation potentials of SOX2/HMGA2-transduced hiNSCs were measured by the percentages of NF-, GFAP-, and O4-positive cells among the total number of nuclei (Figure 3A).

To evaluate the functionality of the hiNSCs, we examined the electrophysiological properties. We observed that hiNSCs generated neurons expressing sodium currents, resulting in multiple action potentials. The sodium current (or inward current) and action potentials were inhibited using the sodium channel blocker lidocaine and restored to normal status after washout (Figures 3B–3D and S3B–S3D). These data revealed that hiNSCs are multipotent, and neurons from hiNSCs showed the functional membrane properties and activities of normal neurons.

Moreover, to investigate whether hiNSCs could also differentiate into three lineages in vivo, CM-DiI-labeled hiNSCs were transplanted into the hippocampal region of 4-week-old mice, followed by immunohistochemical analysis at 3 weeks after transplantation. As expected, some of the grafted hiNSCs differentiated into neurons (CM-DiI$^+$TUJ1$^+$), astrocytes (CM-DiI$^+$GFAP$^+$), or oligodendrocytes (CM-DiI$^+$MBP$^+$) within the brain (indicated with arrows; Figure 3E). We also observed that a few CM-DiI fluorescent cells were negative for these lineage markers (indicated with asterisks), implying that these cells either maintained the NSC status or differentiated into cells positive for other lineage markers, such as PSA-NCAM or DCX (Figures 3E and S3E). Taken together, these results suggest that transplanted hiNSCs survive and differentiate into neurons, astrocytes, and oligodendrocytes in vivo and in vitro.

HMGA2 Facilitates the Efficient Reprogramming of Various Somatic Cells into hiNSCs

We next assessed whether human umbilical cord blood cells (hUCB) could be used as a source for iNSC reprogramming, as, in contrast to fibroblasts, these cells are acquired without invasive procedures and they retain minimal genetic mutations (Broxmeyer et al., 2011; Giorgetti et al., 2012). MSC populations were isolated from hUCBs as previously described (Kim et al., 2013). Following SOX2/HMGA2 transduction, hUCB-MSCs formed networks with colonies at the intersections. hUCB-MSC-derived iNSC colonies appeared at 7–12 days postinfection, and these cells were immunocytochemically demonstrated to be iNSCs through positive staining for PAX6 and NESTIN (Figure 4A). It has been reported that MSCs are positive for CD73 and CD105 but negative for the hematopoietic markers CD34, CD45, and HLA-DR (Dominici et al., 2006). hUCB-MSC-derived

Figure 3. Functional Characterization of SOX2/HMGA2-Transduced hDF-iNSCs In Vitro and In Vivo

(A) Immunocytochemical analysis of hDF-iNSCs (SOX2/HMGA2) after differentiation into three major cell types: neurons (α-internexin, TH, DCX, ChAT, NF, MAP2, and TUJ1), astrocytes (GFAP), and oligodendrocytes (OLIG2 and O4). The scale bars represent 50 or 10 μm. Quantification of neuron, astrocyte, and oligodendrocyte generation was measured according to the NF+, GFAP+, and O4+ cells, respectively, over the total number of cells. Error bars denote the SD of triplicate images.

(B) Representative images of sodium currents and action potential of hiNSC-derived neurons recorded using voltage-clamp readings.

(C) Voltage-clamp recording after blocking sodium currents using lidocaine (0.1%).

(D) Voltage-clamp recording of sodium current restoration after washout.

(E) Transplantation of CM-DiI-labeled hiNSCs into the hippocampal region of 4-week-old mice. hiNSCs were differentiated into neurons (TUJ1), astrocytes (GFAP), and oligodendrocytes (MBP) and colocalized with CM-DiI (arrows). Some hiNSCs showed CM-DiI fluorescence without colocalization (asterisks). The scale bars represent 50 μm.

See also Figure S3.

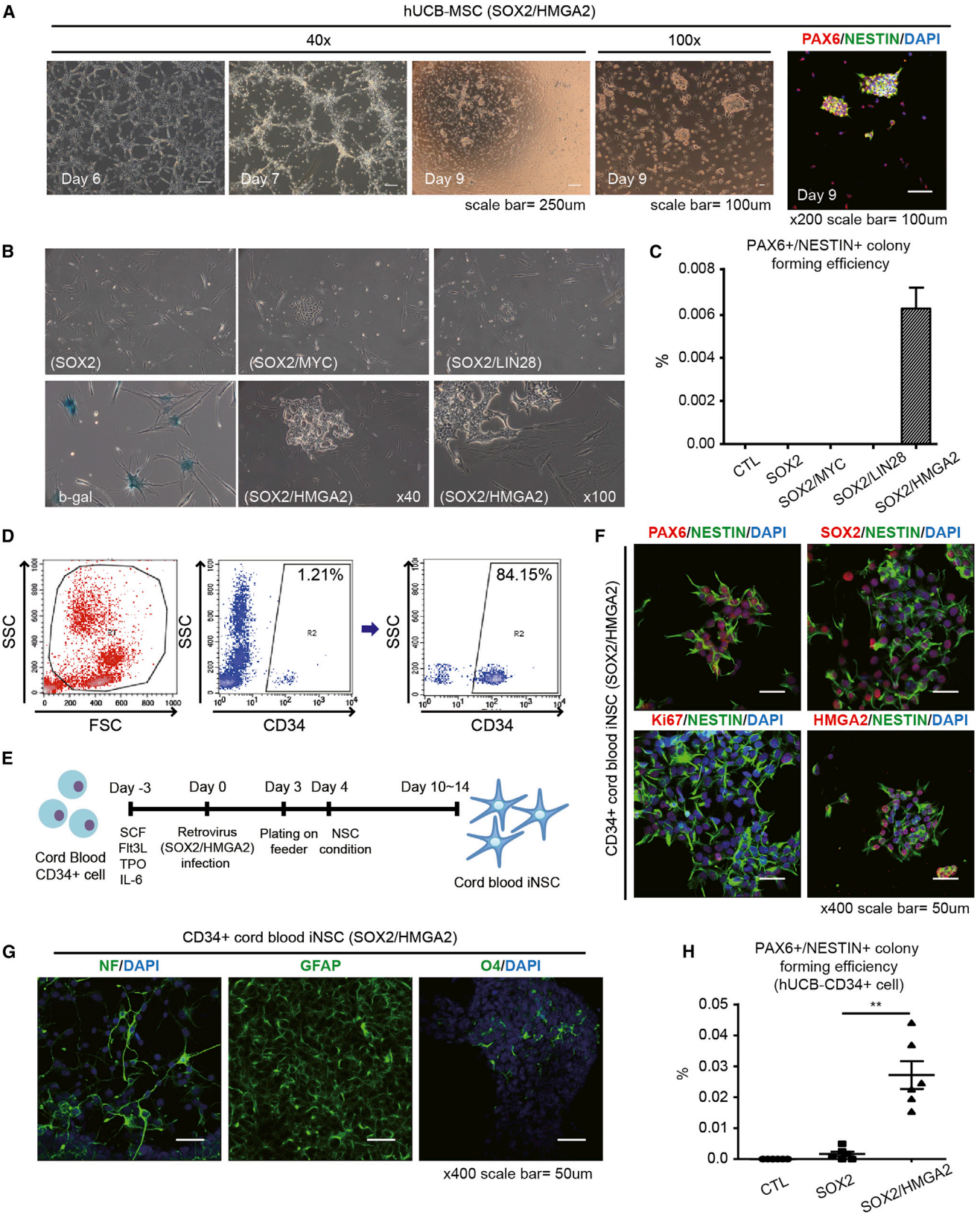

(legend on next page)

iNSCs were negative for CD73 and CD105, suggesting that the cell surface marker signature had changed (Figure S4A). We observed that HMGA2 expression was significantly higher in hUCB-MSCs compared with hDFs (Figure S4B). SOX2/HMGA2-transduced hUCB-MSCs generated 3- to 4-fold more PAX6/NESTIN-positive colonies compared with SOX2-transduced hUCB-MSCs (Figure S4C). To examine the proliferation of H9-NSCs and hiNSC lines derived from different cell sources and combinations of transgenes, we measured the cellular growth rate. We observed that the cellular growth rates of H9-NSCs and hiNSCs were not significantly different, indicating that H9-NSCs and hiNSCs had similar proliferation capacities (Figure S4D).

To explore whether senescent hUCB-MSCs could be induced into neural stem cells, we transduced SOX2 alone or in combination with let-7-targeting factors. To this end, senescent hUCB-MSCs with senescence-associated-β-galactosidase activity were transduced with SOX2, SOX2/MYC, SOX2/LIN28, and SOX2/HMGA2 (Figure 4B). Strikingly, only SOX2/HMGA2 overexpression promoted the formation of hiNSC colonies, whereas SOX2/MYC and SOX2/LIN28 induced morphological changes but did not generate hiNSC colonies (Figure 4B). SOX2/HMGA2 overexpression induced the appearance of two to four colonies from 1×10^5 senescent hUCB-MSCs (conversion efficiency of 0.004–0.008%) at 3 weeks after infection (Figure 4C). Senescent hUCB-MSC-derived iNSCs showed high *SOX2*, *MASH1*, *BLBP*, and *NESTIN* expression, comparable to H9-NSCs (Figure S4F).

We next attempted to generate hiNSCs from the CD34+ fraction of hUCB cells through transduction with SOX2/HMGA2. hUCB CD34+ cells were purified using standard immunomagnetic selection, showing 84.15% purity (Figure 4D). For the stimulation of mitotic division, hUCB CD34+ cells were cultured with cytokines (SCF, Flt3L, TPO, and interleukin-6) for 3 days before retrovirus infection. The cells were subsequently plated onto feeder cells, and 10–14 days after infection, iNSC colonies appeared (Figure 4E). hUCB CD34+ cells did not significantly express NSC or neuron-specific markers, indicating the absence of a neural precursor-like population (Figure S4E). Immunocytochemical staining and RT-PCR revealed that hUCB CD34+ iNSCs were established, showing the positive expression of PAX6, SOX2, Ki67, HMGA2, MASH1, BLBP, and NESTIN (Figures 4F and S4F). Furthermore, these hUCB CD34+ iNSCs developed into neurons, astrocytes and oligodendrocytes (Figure 4G). SOX2 alone was sufficient to generate hUCB CD34+ iNSCs but with low efficiency. Coexpressing SOX2 and HMGA2 in hUCB CD34+ cells increased the frequency of PAX6/NESTIN-positive colony formation 10- to 20-fold (Figure 4H). In summary, efficient direct reprogramming through the synergistic interaction of SOX2 and HMGA2 facilitates the conversion of various somatic cells into hiNSCs.

DISCUSSION

The results obtained in the present study provide compelling evidence that HMGA2/let-7 plays an important role in the direct reprogramming of hDFs, hMSCs, and hUCB CD34+ cells toward hiNSCs and in the maintenance of hiNSC self-renewal. Importantly, the coexpression of SOX2 and HMGA2 significantly shortened the turnaround time and enhanced reprogramming efficiency; thus, cord blood cells or senescent cells can be reprogrammed into hiNSCs. Recent studies have shown that cord-blood-derived CD133+ progenitor cells are converted into neuronal-like cells (CB-iNCs) through the ectopic expression of SOX2 and MYC (Giorgetti et al., 2012). However, CB-iNCs showed limited neuronal differentiation, whereas in the present study, hUCB CD34+ iNSCs showed trilineage neural differentiation potential.

Senescence has been associated with physiological aging, and it has been suggested that this process is a barrier to reprogramming, reflecting a loss of replicative potential and upregulation of cell-cycle-dependent kinase inhibitors (Banito and Gil, 2010). We observed that HMGA2 could overcome senescence-induced barriers, potentially providing a clinical strategy for the production of neural-disease-specific hiNSCs. Because hiNSCs acquire a rejuvenated state and self-renewal, retained toxic or pathogenic metabolites in patient-specific hiNSCs can be diluted, leading to a healthy status more suitable for transplantation (Liu et al., 2012). Therefore, the generation of patient-specific hiNSCs using this protocol might represent a powerful tool for elucidating the molecular mechanisms

Figure 4. Efficient Conversion of Various Somatic Cells with HMGA2

(A) Generation of iNSCs from human-umbilical-cord-blood-derived mesenchymal stem cells with SOX2/HMGA2. Neurosphere-like colonies appeared 7 days after virus transduction. hUCB-MSC-derived iNSCs were immunostained with PAX6 (red), NESTIN (green), and DAPI (blue). The scale bars represent 250 or 100 μm.

(B) Morphology of replicative senescent hUCB-MSCs transduced with SOX2, SOX2/MYC, SOX2/LIN28, or SOX2/HMGA2 after 21 days. Replicative senescent hUCB-MSCs were assessed for β-galactosidase activity. Early iNSC clusters were generated only through SOX2/HMGA2 transduction.

(C) Quantification of the amount of PAX6- and NESTIN-positive colony formation in control and SOX2-, SOX2/MYC-, SOX2/LIN28-, and SOX2/HMGA2-transduced replicative senescent hUCB-MSCs. Error bars denote the SD of triplicate assays.

(D) Representative dot plot images for the purity of CD34+ cells through a flow cytometric analysis. The cells were 84.15% positive for CD34 after sorting from mononuclear cells. FSC, forward scatter; SSC, side scatter.

(E) Schematic presentation of the strategy for reprogramming hUCB-CD34+ cells into hiNSCs.

(F) Characterization of hUCB-CD34+ iNSCs (SOX2/HMGA2) using immunocytochemistry. The cells were stained for the NSC-specific markers PAX6, HMGA2, NESTIN, and SOX2 and a proliferation marker, Ki67. The scale bars represent 50 μm.

(G) Immunocytochemical analysis of hUCB-CD34+ iNSCs (SOX2/HMGA2) after differentiation into three major cell types: neurons (NF); astrocytes (GFAP); and oligodendrocytes (O4). The scale bars represent 50 μm.

(H) The efficiency of PAX6- and NESTIN-positive colony formation was measured in control hUCB-CD34+ cells, SOX2-, and SOX2/HMGA2-transduced hUCB-CD34+ cells. Error bars denote the SD of six separate assays. $^{**}p < 0.01$.

See also Figure S4.

underlying neural diseases and might have implications for therapeutic applications.

To obtain deeper insight into the role of let-7, known targets of let-7, MYC, LIN28, and HMGA2 were overexpressed together with SOX2 (Mayr et al., 2007; Rybak et al., 2008; Sampson et al., 2007). Although these factors showed a positive regulation of colony formation, the effect of each factor on proliferation was inconsistent with colony formation (Figure 2), suggesting that each factor has a different mechanistic function in reprogramming in addition to the increase in proliferation. This idea is supported by other reports that MYC, a well-known proliferation stimulator (Dang, 2012), promotes the transcription of active genes (Lin et al., 2012; Nie et al., 2012). LIN28 assists iPSC formation, depending on the acceleration of the division rate (Hanna et al., 2009). Nonetheless, HMGA2 showed the most-efficient reprogramming into iNSCs, although it showed the least-proliferative potential, suggesting that HMGA2 retains far more mechanistic potential for iNSC reprogramming than other factors.

HMGA2 can be a potent regulator of higher-order chromatin compaction during reprogramming. Indeed, the compact chromatin structure induced through the linker histone H1 interferes with the pluripotency of embryonic stem cells (ESCs) and efficiency of iPSC reprogramming (Gaspar-Maia et al., 2009; Zhang et al., 2012). The conversion of the chromatin structure into a global open state through competition with the linker histone H1 might be closely associated with the positive effect of HMGA2 on hiNSC derivation (Catez et al., 2004; Kishi et al., 2012). Moreover, we found that HMGA2 facilitates a high self-renewal and neurogenic capacity in hiNSCs, consistent with the reports that HMGA2 is a key factor for sustaining early-stage neural stem cells during development (Kishi et al., 2012; Miller and Gauthier, 2007).

Furthermore, in the present study, we showed that hUCB-derived MSCs express substantially higher levels of HMGA2 than hDFs and are more prone to reprogramming into iNSCs (Figure S4). Upregulated HMGA2 levels might reflect the higher reprogramming efficiency of MSCs into iPSCs (Sugii et al., 2010; Sun et al., 2009) or iNSCs compared with fibroblasts. These reports suggest that HMGA2 is a contributor to SOX2-mediated iNSC reprogramming through mechanistic regulation. Thus, it will be worthwhile to determine the mechanism underlying the regulatory role of HMGA2 during reprogramming in future studies.

EXPERIMENTAL PROCEDURES

Cell Derivation, Generation, and Viral Infection

hUCB-MSCs and hUCB CD34+ cells were isolated as previously described (Kim et al., 2013). Briefly, hUCB-MSCs were obtained from the umbilical cord blood (UCB) of 20- to 30-year-old mothers immediately after full-term delivery; the mothers were informed of the UCB procedure. Blood samples collected within 24 hr were used. After the UCB samples were mixed with HetaSep solution (Stem Cell Technology) at a ratio of 5:1 (v/v), the mixture was incubated at room temperature until the red blood cells were depleted. The supernatant was carefully collected, and the mononuclear cells were isolated through a Ficoll (GE Healthcare Life Sciences) density-gradient centrifugation at 2,500 rpm for 20 min. The cells were washed twice with PBS and seeded onto culture dishes containing growth media. The isolation and research protocols were approved by the Boramae Hospital Institutional Review Board (IRB) and the IRB of Seoul National University (1109/001-006).

The commercial cell line hDFs (Life Technologies) were purchased. Retrovirus was produced as previously described (Yu et al., 2012). To generate iNSCs, retroviral factors, *SOX2*, *HMGA2*, *MYC*, and *LIN28* were transduced into hDFs, hUCB-MSCs, and hUCB CD34+ cells. After expansion of the cells, medium was changed to the NSC maintenance medium with growth factors. NSC-like colonies were collected and transferred to neurosphere culture condition. Cells were cultured as neurosphere and grown as attached cells on PLO/FN-coated dishes, repeatedly. More detailed information can be found in the Supplemental Experimental Procedures.

microRNA Microarray Analysis

Total RNA was extracted from the cells using Trizol reagent; 100 ng of total RNA was labeled and hybridized using the Agilent miRNA Complete Labeling and Hyb Kit to generate fluorescently labeled miRNAs according to the manufacturer's instructions. The labeled miRNA signals were scanned using an Agilent microarray scanner. Raw data (GEO accession number: GSE59301) were extracted using the software provided by Agilent Feature Extraction Software (v11.0.1.1). The raw data for the same gene were then summarized automatically in Agilent feature extraction protocol to generate Gene view file, which provided expression data for each gene probed on the array.

Array data were filtered by gIsGeneDetected = 1 in all samples (1: detected).

Selected miRNA gtotalGeneSignal value was transformed by logarithm and normalized by quantile method. The comparative analysis between test sample and control sample was carried out using fold change.

All data analysis and visualization of differentially expressed genes was conducted using R statistical language v. 2.15.0.

Quantitative Real-Time PCR

Total RNA was extracted from cells using TRIzol reagent according to the manufacturer's instructions. cDNA was synthesized using the Superscript III First-Strand Synthesis System (Invitrogen). Real-time PCR was performed using SYBR Green PCR Master Mix (Applied Biosystems). ABI 7300 sequence detection system with supplied software (Applied Biosystems) was used to quantify gene expression. Each gene was normalized to *GAPDH* as a housekeeping control, and gene expression levels were measured in at least three independent analyses. Primers used for qRT-PCR are provided in Table S1.

In Vitro Differentiation

For neural differentiation, iNSCs were seeded at a density of 1,000 cells/well onto poly-L-ornithine/fibronectin-coated coverslips in 24-well plates containing iNSC maintenance medium (ReNcell NSC maintenance media; Millipore). After 24 hr, the medium was changed to Neurocult (Stem Cell Technology) for random differentiation. After 1 week of differentiation in Neurocult, the medium was changed for the induction of three specific lineages (neuron, astrocyte, and oligodendrocyte). The neuronal induction medium contained a 1:1 mixture of Neurobasal medium (GIBCO BRL) and Dulbecco's modified Eagle's medium (DMEM)/F12 medium (GIBCO BRL) supplemented with B27 (GIBCO BRL), Gmax (GIBCO BRL), retinoic acid (RA) (Sigma), ascorbic acid (Sigma), brain-derived neurotrophic factor (Peprotech), glial-cell-line-derived neurotrophic factor (Peprotech), and forskolin (Sigma). The astrocyte induction medium contained DMEM (high glucose) supplemented with N2 (GIBCO BRL), Gmax, and 1% fetal bovine serum. Two types of oligodendrocyte induction media were used as previously described (Hu et al., 2009). DMEM/F12 supplemented with N2, MEM nonessential amino acids solution (MEM NEAA)(GIBCO BRL), heparin (Sigma), RA, sonic hedgehog (Peprotech), and B27 was used for 2 weeks and was subsequently changed to DMEM/F12 supplemented with N2, B27, MEM NEAA, T3, cyclic AMP (Sigma), platelet-derived growth factor (Peprotech), insulin-like growth factor (R&D Systems), and neurotrophin-3 (Sigma) for 2 weeks.

Patch-Clamp Reading

Whole-cell patch-clamp recordings in neurons derived from iNSCs were performed using an EPC 10 USB amplifier (HEKA Electronik) at room temperature (22°C ± 1°C). The recording chamber was filled with continuously flowing Tyrode solution (flow rate: 10 ml/min). Patch electrodes were generated

from borosilicate glass capillaries using a PC-10 puller (Narishige Company). The resistance of the electrode was 4–7 MΩ when filled with pipette solution. The data were acquired and analyzed using the Pulse program version 8.67 (HEKA Electronik) and Origin 6.1 software (MicroCal). The current was filtered at 3 kHz using a four-pole Bessels filter and digitized at 10 kHz. Tyrode solution contained 143 mM NaCl, 5.4 mM KCl, 0.5 mM MgCl2, 1.8 mM CaCl2, 0.5 mM NaHPO4, 10 mM glucose, and 5 mM 4-(2-hydroxyethyl)-1-piperazineethanesulfonic acid (HEPES), and the pH was adjusted to 7.5 with NaOH. The pipette solution contained 150 mM KCl, 1.0 mM MgCl2, 10 mM HEPES, 5 mM EGTA, and 2 mM Mg-ATP, and the pH was adjusted to 7.2 with NaOH. Lidocaine (0.1%) was used to block the Na current.

Transplantation of the hiNSCs into Mice

The hiNSCs were detached from culture dishes by using Accutase. The hiNSCs were labeled and suspended in PBS. Balb/c mice were obtained from Jackson Laboratory. Mice were group housed in the animal facility of Seoul National University. All experiments were approved by and followed the regulations of the Institute of Laboratory Animals Resources (SNU-120821-5). Four-week-old mice were anesthetized, and labeled cells were transplanted into hippocampal regions. After 3 weeks, mice were sacrificed and brain was isolated. After cryosectioning, immunohistochemistry was performed to trace the transplanted hiNSCs and differentiated hiNSCs that integrated into mice brain. More detailed information can be found in the Supplemental Experimental Procedures.

ACCESSION NUMBERS

The human miRNA microarray data are available in the Gene Expression Omnibus database (http://www.ncbi.nlm.nih.gov/gds) under the accession number GSE59301.

SUPPLEMENTAL INFORMATION

Supplemental Information includes Supplemental Experimental Procedures, four figures, and one table and can be found with this article online at http://dx.doi.org/10.1016/j.celrep.2014.12.038.

AUTHOR CONTRIBUTIONS

K.-S.K. and K.-R.Y. conceived the research. K.-R.Y., J.-H.S., and J.-J.K. designed and analyzed the research. K.-R.Y., J.-H.S., J.-J.K., M.G.K., J.Y.L., S.W.C., H.-S.K., Y.S., S.L., T.S., and M.K.J. performed the experiment. S.J.J. performed the electrophysiology. D.-W.K., S.J.J., S.S., and D.W.H. advised the research. K.-S.K., K.-R.Y., J.-H.S., and J.-J.K. wrote the manuscript.

ACKNOWLEDGMENTS

We are extremely grateful to Dr. Kwang-Soo Kim (Harvard Medical School) for crucial advice and discussions. This research was supported by the Bio and Medical Technology Development Program of the National Research Foundation (NRF) funded by the Ministry of Science, ICT and Future Planning (2012M3A9C7050126) to D.-W.K. and the Research Institute for Veterinary Science, Seoul National University.

Received: July 11, 2014
Revised: October 13, 2014
Accepted: December 16, 2014
Published: January 15, 2015

REFERENCES

Banito, A., and Gil, J. (2010). Induced pluripotent stem cells and senescence: learning the biology to improve the technology. EMBO Rep. *11*, 353–359.

Broxmeyer, H.E., Lee, M.R., Hangoc, G., Cooper, S., Prasain, N., Kim, Y.J., Mallett, C., Ye, Z., Witting, S., Cornetta, K., et al. (2011). Hematopoietic stem/progenitor cells, generation of induced pluripotent stem cells, and isolation of endothelial progenitors from 21- to 23.5-year cryopreserved cord blood. Blood *117*, 4773–4777.

Catez, F., Yang, H., Tracey, K.J., Reeves, R., Misteli, T., and Bustin, M. (2004). Network of dynamic interactions between histone H1 and high-mobility-group proteins in chromatin. Mol. Cell. Biol. *24*, 4321–4328.

Copley, M.R., Babovic, S., Benz, C., Knapp, D.J., Beer, P.A., Kent, D.G., Wohrer, S., Treloar, D.Q., Day, C., Rowe, K., et al. (2013). The Lin28b-let-7-Hmga2 axis determines the higher self-renewal potential of fetal haematopoietic stem cells. Nat. Cell Biol. *15*, 916–925.

Dang, C.V. (2012). MYC on the path to cancer. Cell *149*, 22–35.

Dominici, M., Le Blanc, K., Mueller, I., Slaper-Cortenbach, I., Marini, F., Krause, D., Deans, R., Keating, A., Prockop, Dj., and Horwitz, E. (2006). Minimal criteria for defining multipotent mesenchymal stromal cells. The International Society for Cellular Therapy position statement. Cytotherapy *8*, 315–317.

Fusco, A., and Fedele, M. (2007). Roles of HMGA proteins in cancer. Nat. Rev. Cancer *7*, 899–910.

Gaspar-Maia, A., Alajem, A., Polesso, F., Sridharan, R., Mason, M.J., Heidersbach, A., Ramalho-Santos, J., McManus, M.T., Plath, K., Meshorer, E., and Ramalho-Santos, M. (2009). Chd1 regulates open chromatin and pluripotency of embryonic stem cells. Nature *460*, 863–868.

Giorgetti, A., Marchetto, M.C., Li, M., Yu, D., Fazzina, R., Mu, Y., Adamo, A., Paramonov, I., Cardoso, J.C., Monasterio, M.B., et al. (2012). Cord blood-derived neuronal cells by ectopic expression of Sox2 and c-Myc. Proc. Natl. Acad. Sci. USA *109*, 12556–12561.

Han, D.W., Tapia, N., Hermann, A., Hemmer, K., Höing, S., Araúzo-Bravo, M.J., Zaehres, H., Wu, G., Frank, S., Moritz, S., et al. (2012). Direct reprogramming of fibroblasts into neural stem cells by defined factors. Cell Stem Cell *10*, 465–472.

Hanna, J., Saha, K., Pando, B., van Zon, J., Lengner, C.J., Creyghton, M.P., van Oudenaarden, A., and Jaenisch, R. (2009). Direct cell reprogramming is a stochastic process amenable to acceleration. Nature *462*, 595–601.

Hu, B.Y., Du, Z.W., and Zhang, S.C. (2009). Differentiation of human oligodendrocytes from pluripotent stem cells. Nat. Protoc. *4*, 1614–1622.

Kawahara, H., Imai, T., and Okano, H. (2012). MicroRNAs in neural stem cells and neurogenesis. Front. Neurosci. *6*, 30.

Kim, H.S., Shin, T.H., Lee, B.C., Yu, K.R., Seo, Y., Lee, S., Seo, M.S., Hong, I.S., Choi, S.W., Seo, K.W., et al. (2013). Human umbilical cord blood mesenchymal stem cells reduce colitis in mice by activating NOD2 signaling to COX2. Gastroenterology *145*, 1392–1403.

Kishi, Y., Fujii, Y., Hirabayashi, Y., and Gotoh, Y. (2012). HMGA regulates the global chromatin state and neurogenic potential in neocortical precursor cells. Nat. Neurosci. *15*, 1127–1133.

Lin, C.Y., Lovén, J., Rahl, P.B., Paranal, R.M., Burge, C.B., Bradner, J.E., Lee, T.I., and Young, R.A. (2012). Transcriptional amplification in tumor cells with elevated c-Myc. Cell *151*, 56–67.

Liu, G.H., Yi, F., Suzuki, K., Qu, J., and Izpisua Belmonte, J.C. (2012). Induced neural stem cells: a new tool for studying neural development and neurological disorders. Cell Res. *22*, 1087–1091.

Mayr, C., Hemann, M.T., and Bartel, D.P. (2007). Disrupting the pairing between let-7 and Hmga2 enhances oncogenic transformation. Science *315*, 1576–1579.

Miller, F.D., and Gauthier, A.S. (2007). Timing is everything: making neurons versus glia in the developing cortex. Neuron *54*, 357–369.

Nie, Z., Hu, G., Wei, G., Cui, K., Yamane, A., Resch, W., Wang, R., Green, D.R., Tessarollo, L., Casellas, R., et al. (2012). c-Myc is a universal amplifier of expressed genes in lymphocytes and embryonic stem cells. Cell *151*, 68–79.

Nishino, J., Kim, I., Chada, K., and Morrison, S.J. (2008). Hmga2 promotes neural stem cell self-renewal in young but not old mice by reducing p16Ink4a and p19Arf Expression. Cell *135*, 227–239.

Reeves, R. (2001). Molecular biology of HMGA proteins: hubs of nuclear function. Gene *277*, 63–81.

Ring, K.L., Tong, L.M., Balestra, M.E., Javier, R., Andrews-Zwilling, Y., Li, G., Walker, D., Zhang, W.R., Kreitzer, A.C., and Huang, Y. (2012). Direct reprogramming of mouse and human fibroblasts into multipotent neural stem cells with a single factor. Cell Stem Cell *11*, 100–109.

Rybak, A., Fuchs, H., Smirnova, L., Brandt, C., Pohl, E.E., Nitsch, R., and Wulczyn, F.G. (2008). A feedback loop comprising lin-28 and let-7 controls pre-let-7 maturation during neural stem-cell commitment. Nat. Cell Biol. *10*, 987–993.

Sampson, V.B., Rong, N.H., Han, J., Yang, Q., Aris, V., Soteropoulos, P., Petrelli, N.J., Dunn, S.P., and Krueger, L.J. (2007). MicroRNA let-7a down-regulates MYC and reverts MYC-induced growth in Burkitt lymphoma cells. Cancer Res. *67*, 9762–9770.

Sugii, S., Kida, Y., Kawamura, T., Suzuki, J., Vassena, R., Yin, Y.Q., Lutz, M.K., Berggren, W.T., Izpisúa Belmonte, J.C., and Evans, R.M. (2010). Human and mouse adipose-derived cells support feeder-independent induction of pluripotent stem cells. Proc. Natl. Acad. Sci. USA *107*, 3558–3563.

Sun, N., Panetta, N.J., Gupta, D.M., Wilson, K.D., Lee, A., Jia, F., Hu, S., Cherry, A.M., Robbins, R.C., Longaker, M.T., and Wu, J.C. (2009). Feeder-free derivation of induced pluripotent stem cells from adult human adipose stem cells. Proc. Natl. Acad. Sci. USA *106*, 15720–15725.

Thier, M., Wörsdörfer, P., Lakes, Y.B., Gorris, R., Herms, S., Opitz, T., Seiferling, D., Quandel, T., Hoffmann, P., Nöthen, M.M., et al. (2012). Direct conversion of fibroblasts into stably expandable neural stem cells. Cell Stem Cell *10*, 473–479.

Xue, Y., Ouyang, K., Huang, J., Zhou, Y., Ouyang, H., Li, H., Wang, G., Wu, Q., Wei, C., Bi, Y., et al. (2013). Direct conversion of fibroblasts to neurons by reprogramming PTB-regulated microRNA circuits. Cell *152*, 82–96.

Yoo, A.S., Sun, A.X., Li, L., Shcheglovitov, A., Portmann, T., Li, Y., Lee-Messer, C., Dolmetsch, R.E., Tsien, R.W., and Crabtree, G.R. (2011). MicroRNA-mediated conversion of human fibroblasts to neurons. Nature *476*, 228–231.

Yu, K.R., Yang, S.R., Jung, J.W., Kim, H., Ko, K., Han, D.W., Park, S.B., Choi, S.W., Kang, S.K., Schöler, H., and Kang, K.S. (2012). CD49f enhances multipotency and maintains stemness through the direct regulation of OCT4 and SOX2. Stem Cells *30*, 876–887.

Yu, K.R., Park, S.B., Jung, J.W., Seo, M.S., Hong, I.S., Kim, H.S., Seo, Y., Kang, T.W., Lee, J.Y., Kurtz, A., and Kang, K.S. (2013). HMGA2 regulates the in vitro aging and proliferation of human umbilical cord blood-derived stromal cells through the mTOR/p70S6K signaling pathway. Stem Cell Res. (Amst.) *10*, 156–165.

Yuan, S.H., Martin, J., Elia, J., Flippin, J., Paramban, R.I., Hefferan, M.P., Vidal, J.G., Mu, Y., Killian, R.L., Israel, M.A., et al. (2011). Cell-surface marker signatures for the isolation of neural stem cells, glia and neurons derived from human pluripotent stem cells. PLoS ONE *6*, e17540.

Zhang, Y., Cooke, M., Panjwani, S., Cao, K., Krauth, B., Ho, P.Y., Medrzycki, M., Berhe, D.T., Pan, C., McDevitt, T.C., and Fan, Y. (2012). Histone h1 depletion impairs embryonic stem cell differentiation. PLoS Genet. *8*, e1002691.

Zhao, C., Sun, G., Li, S., Lang, M.F., Yang, S., Li, W., and Shi, Y. (2010). MicroRNA let-7b regulates neural stem cell proliferation and differentiation by targeting nuclear receptor TLX signaling. Proc. Natl. Acad. Sci. USA *107*, 1876–1881.